

Anomalous transport of particle tracers in multidimensional cellular flows

W. L. Vargas,* L. E. Palacio, and D. M. Dominguez

School of Engineering, Universidad Militar Nueva Granada, Bogota, Colombia

(Received 7 October 2002; published 26 February 2003)

Advection of tracers is studied numerically in time-dependent, two-dimensional cellular flows and a time-independent, three-dimensional cellular flow field. Tracers in these flows follow trajectories that are either periodic or chaotic and mimic correlated Lévy flights. The probability density function of displacements for particles in the ordered regions of the flow follows a classical Gaussian dispersion process. The particle trajectories in the chaotic regions of the flow exhibit anomalous diffusion and the probability density function of displacements is well modeled by a time-fractional diffusion equation of order α . The overall process of particle dispersion is found to be controlled mainly by the chaotic regions within the flow field. From the perspective of Lagrangian dynamics our results indicate that the advection of particles in flow fields prone to exhibit chaotic advection is a combination of both classical, i.e., Gaussian, behavior and anomalous, i.e., non-Gaussian, diffusion.

DOI: 10.1103/PhysRevE.67.026314

PACS number(s): 47.52.+j, 05.40.-a, 05.45.-a

I. INTRODUCTION

Particle transport has been of interest for decades because of its prevalence in science and engineering applications. In the last few decades, advection experiments on prototypical flows have provided an appropriate model for the understanding of dynamical systems. One important observation common to these studies has been that many simple velocity fields can generate complicated fluid particle trajectories, thus resulting in what is now known as chaotic advection, Lagrangian turbulence, or Lagrangian chaos [1,2]. Chaotic advection defines a kinematic phenomenon in which the motion of the particle tracers is chaotic—in a Lagrangian sense—even though the velocity field may be regular—in the Eulerian sense—and nonturbulent [3]. Lagrangian chaos has been shown to occur in three-dimensional time-independent flows [1,4] and two-dimensional time-dependent flows [5]. This process has also been found to significantly enhance long-range transport [1,3,6-8] via enhanced mixing and/or anomalous diffusion. Chaotic advection enhances mixing, since one of the key signatures of chaos is the exponential separation of initially close points [9]. Anomalous diffusion appears due to inhomogeneities in the flow field, regular or coherent regions, and the shear flow, that cause particles to spend time moving either too slow or too fast [10].

The motion of passive particles in prototype chaotic flow fields has been the subject of several investigations both experimental (e.g., Solomon and Gollub [11,12], Weeks [13], Fountain *et al.* [14,15]) and numerical (e.g., Tsega *et al.* [16], del Castillo-Negrete [10], Newton and Meiburg [2], Weiss *et al.* [17]). These studies conducted in both two- and three-dimensional flows have shown that the dynamics of these flows can be very complex. Nested Kolmogorov-Arnold-Moser KAM tori, cantori, and periodic islands are found embedded within the flow field. Chaotic advection studies in three-dimensional flows are less common. The reason is the

lack of a test-bed three-dimensional flow field with enough engineering relevance and amenable to both experimental and numerical treatment [14,15]. The existing three-dimensional studies have used mathematical models which include *ABC* flow [18], two chains of alternating vortices [6], steady Stokes flow within a spherical drop [19,20], Taylor-Couette flow [21], and the partitioned-pipe mixer [22]. In many of the flows mentioned above, it has been found that correlations in time and/or space cause anomalous transport whose probability density function (PDF) deviates from the classical Gaussian behavior and/or whose mean square displacement is nonlinear in the long-time limit, i.e., $\sigma^2 \propto t^\gamma$, with $\gamma \neq 1$. Fractional diffusion equations aimed at describing this anomalous behavior have recently been employed to investigate phenomena ranging from advection of particle tracers in porous media [23], fractional Brownian motion [24], anomalous diffusion with adsorption [25], and fractional heat conduction [26] to tracer advection [27]. Closely related models have also been extensively used in the description of economic time series and market dynamics [28,29].

As we show below, the Lagrangian dynamics of cellular flows display properties of both classical (Gaussian) and non-Gaussian (anomalous) systems, which can be described by applying the tools of fractional calculus in the description of the particle displacements. The remainder of this paper is organized as follows. Section II introduces the velocity fields used in the study. The statistical tools for Lagrangian analysis are considered in Sec. III. In Sec. IV we discuss the statistical properties of the particle trajectories in the flow fields under study. Finally, in Sec. V we provide conclusions and perspectives.

II. LAGRANGIAN FORMULATION OF TRACER MOTION

In this article, we report on a simulation study of tracer advection in three different cellular flow fields and the Lagrangian analysis of the particle displacements using a fractional diffusion equation. The numerical experiments are performed in well established prototypical flows such as the

*Corresponding author. Electronic address: wvargas@007mundo.com

“Kelvin cat eyes” flow, the Rayleigh-Bénard flow, and a three-dimensional flow recently introduced by Fogleman *et al.* [6]. This three-dimensional flow is composed of the superposition of two chains of alternating vortices, one horizontal and the other vertical. These flows are ideal for this study partly because of their simplicity and the rich transport properties which have been found [6,16,30] and partly because of the possibility of experimental verification of the estimated behavior. This study is similar in spirit to earlier studies of tracer advection by prototype flow fields tuned to model chaotic advection, but differs primarily in the fact that tools from *fractional calculus* are used to describe the probability density function of the tracer displacements. Passive tracers are placed in the flow and their behavior under a chosen set of flow parameters is studied. A fourth-order Runge-Kutta method with a time step value of 10^{-4} was employed to numerically integrate the differential equations that make up the velocity field. It is important to note that using a sufficiently small time increment is essential for resolving important features of the Poincaré sections, such as KAM tori and cantori.

A. Kelvin cat eyes flow

This flow is based on the family of solutions to the steady Euler equations known as the Stuart vortices. The stream function for the “Kelvin cat eyes” flow is given as follows:

$$\Psi(x,y,t) = Uy + \left[\frac{\Delta U h}{2} \ln \left[\cosh \left(\frac{y}{h} \right) + A \cos \left(\frac{x - Ut}{h} \right) \right] \right]. \quad (1)$$

This stream function represents a train of vortices moving in the x direction. It is a steady solution of the two-dimensional Euler equation and has a 2π periodicity in the x direction [16]. The nondimensional parameter A represents the strength of the vorticity. For the purpose of this study, the value of A was set at a constant value of 0.8 [16]. The parameter h represents the distance between two adjacent vortices. The stream function in Eq. (1) describes a velocity field given by

$$\frac{\partial \Psi}{\partial y} = \frac{dx}{dt} = \frac{\sinh y}{\cosh y + A \cos x} + \epsilon \sin(\omega t), \quad (2)$$

$$-\frac{\partial \Psi}{\partial x} = -\frac{dy}{dt} = -\frac{A \sin x}{\cosh y + A \cos x} + \epsilon \sin(\omega t). \quad (3)$$

Here ϵ represents the perturbation constant and ω describes the driving frequency. Figure 1 illustrates the trajectories of 10 000 tracer particles advected in a Stuart vortex.

Transport and mixing in the time-periodic Kelvin cat eyes flow has been investigated by Ottino [31] and Tsega *et al.* [16], where mixing was analyzed for various values of the driving frequency and perturbation constant. Numerical and experimental studies of advection have been reported by del Castillo Negrete [10] and Weeks [13], among others. Lagrangian dynamics of aerosol and bubble particles has also been examined in this flow [16].

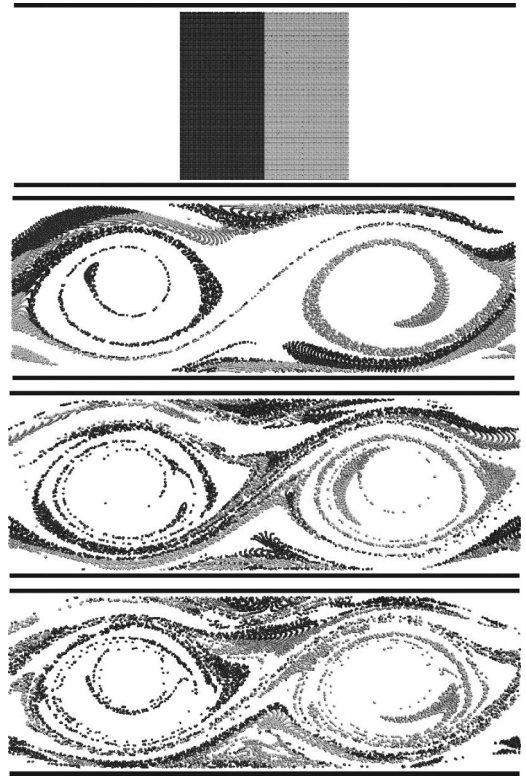


FIG. 1. Poincaré plots of the advection process of 10 000 colored particles in a Kelvin cat eyes flow. $\epsilon=0.1$, $\omega=1.2$, $A=0.8$.

B. Rayleigh-Bénard flow

This flow is a particularly simple two-dimensional time-dependent flow. It is composed of an oscillating vortex chain which has been aptly explored as a simple model of time-periodic Rayleigh-Bénard (RB) convection. The equations describing this flow are as follows:

$$\frac{\partial \Psi}{\partial y} = \frac{dx}{dt} = -a \frac{\lambda}{2d} \cos \left[\frac{2\pi[x + B \sin(\omega t)]}{\lambda} \right] \sin \left(\frac{\pi y}{d} \right), \quad (4)$$

$$-\frac{\partial \Psi}{\partial x} = -\frac{dy}{dt} = a \sin \left[\frac{2\pi[x + B \sin(\omega t)]}{\lambda} \right] \cos \left(\frac{\pi y}{d} \right). \quad (5)$$

In these equations, a is the maximum speed, d is the vortex height, λ is the wavelength of the vortex chain, and B represents the amplitude of the lateral oscillations. Figure 2 shows the advection of 14 000 particles at a frequency $\omega = 0.1$. Qualitatively, the behavior seen in the simulation is similar to that observed in experiments; see, e.g., Fig. 3 in, [32].

Numerical and experimental studies of advection in Rayleigh-Bénard flow have been reported by Camassa and Wiggins [30], Solomon and Gollub [11,12], Solomon *et al.* [32], and Castiglione *et al.* [33], among others.

C. Three-dimensional vortex flow

A three-dimensional flow has recently been introduced by Fogleman *et al.* [6]. The flow is the superposition of two chains of alternating vortices. The equations describing the velocity field are

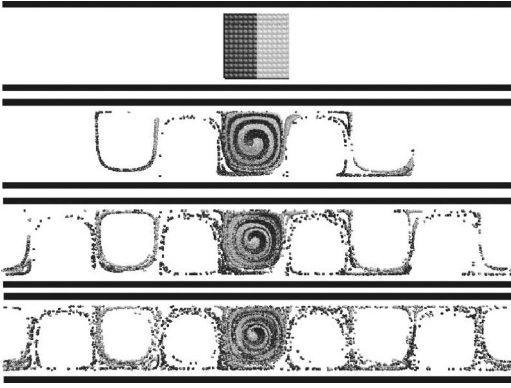


FIG. 2. Poincaré plots of the advection process of 14 000 colored particles in a Rayleigh-Bénard flow. Snapshots taken every period of oscillation. $B=0.1$, $a=d=1.0$, $\lambda=2d$, $\omega=0.1$.

$$\frac{dx}{dt} = -a_1 \frac{\lambda}{2d_1} \cos\left[\frac{2\pi(x+0.5)}{\lambda}\right] \sin\left(\frac{\pi y}{d_1}\right) - a_2 \frac{\lambda}{2d_2} \cos\left[\frac{2\pi x}{\lambda}\right] \sin\left(\frac{\pi z}{d_2}\right), \quad (6)$$

$$\frac{dy}{dt} = a_1 \sin\left[\frac{2\pi(x+0.5)}{\lambda}\right] \cos\left(\frac{\pi y}{d_1}\right), \quad (7)$$

$$\frac{dz}{dt} = a_2 \sin\left[\frac{2\pi x}{\lambda}\right] \cos\left(\frac{\pi z}{d_2}\right). \quad (8)$$

In these equations, a_1 and a_2 indicate the magnitudes of the two overlapping vortex chains, and d_1 and d_2 are the width and height of the fluid layer, respectively. For the purpose of this study, all the vortices are assumed to have aspect ratio $d_1/d_2=1.0$ and $\lambda=2.0$. The relative magnitude of the overlapping is characterized by the ratio a_1/a_2 . Unless indicated otherwise, the ratio a_1/a_2 is kept at a constant value of 5.0. A snapshot of the flow is illustrated in Fig. 3. The points in this figure show the x - y - z coordinates of 20 000 tracer particles. Periodic boundary conditions have been imposed.

A numerical study of long-range transport in three-dimensional (3D) vortex flow was conducted by Fogleman *et al.* [6]. Their findings can be summarized as follows. The variance growth of particle ensembles for both amplitude

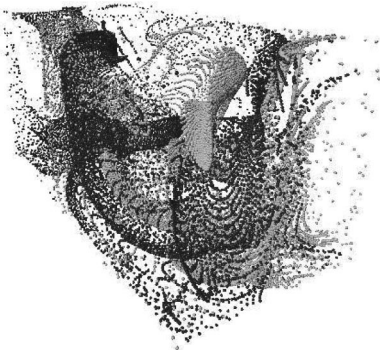


FIG. 3. Snapshot of the advection process of 20 000 colored particles in a 3D vortex flow. $a_1/a_2=1.0$, $d_1/d_2=1.0$, $\lambda=2.0$.

ratios considered, $a_1/a_2=5.0$ and $a_1/a_2=1.0$, exhibit two behaviors: a transient and a long-term regime. According to the results the transient regime can exhibit diffusive or ballistic behavior depending on the value of the ratio a_1/a_2 . The long-term behavior is in both cases superdiffusive (i.e., $\sigma^2 \propto t^\gamma$). The PDFs of flight lengths for both amplitude ratios exhibit tail decay consistent with the definition of Lévy flight.

III. LAGRANGIAN ANALYSIS

The results of a Lagrangian dynamical analysis are usually presented in terms of the particle displacements $\sigma^2 = \langle (x[t] - x[0])^2 \rangle$ and the probability density function of particle ensembles. If classical behavior holds one has $\langle (x[t] - x[0])^2 \rangle \approx 2Dt$. The tracer behaves like a Brownian particle. However, there exist cases where anomalous diffusion is observed (by anomalous we mean non-Gaussian), i.e., $\langle (x[t] - x[0])^2 \rangle \propto t^\gamma$ with $\gamma \neq 1$. The case $\gamma < 1$ determines a subdiffusive system while $\gamma > 1$ corresponds to superdiffusion [10,33]. If the system exhibits anomalous behavior, the probability density function of particle displacements δx , $P(\delta x, t)$, is asymmetric and broader than the classical Gaussian distribution. For weak anomalous diffusion [33], the long-term distribution is of the form $t^{-\gamma} F(X/t^\gamma)$, where $X = \delta x - \langle \delta x \rangle$, F is a scaling function which in general is different from Gaussian, and γ is the anomalous diffusion exponent, which is a measure of the long-range memory of the displacements. As a result of this behavior the variance scales as $\sigma^2 \propto t^\gamma$. According to the central limit theorem, transport in the long-time limit $t \rightarrow \infty$ will be diffusive with $\gamma=1.0$. On the other hand, if superdiffusivity is present, $\gamma > 1.0$; subdiffusivity will occur otherwise. Trapping is the mechanism that leads to subdiffusion whereas superdiffusion is possible if the trajectories are characterized by long “jumps.” It is important to note that asymmetry, diffusion exponents $\gamma > 1.0$, and therefore anomalous behavior, has been previously observed in all the flows considered in this study.

One of the most basic problems in transport is that of the study of the long-term behavior of σ^2 , and of the probability density function of particle displacements, $P(\delta x, t)$. A common approach is to assume that at long times $P(\delta x, t)$ is a Gaussian distribution that evolves in time according to the well known diffusion equation given by

$$\frac{\partial P}{\partial t} = \mathcal{D} \frac{\partial^2 P}{\partial x^2}, \quad (9)$$

where \mathcal{D} is the diffusivity, which satisfies the condition $\mathcal{D} = \lim_{t \rightarrow \infty} \sigma^2/2t$. The solution to Eq. (9) with initial condition $P(\delta x, 0) = \delta(x)$ is well known:

$$P(\delta x, t) = \frac{1}{\sqrt{4\mathcal{D}\pi t}} \exp\left[-\frac{\delta x^2}{4\mathcal{D}t}\right] \quad (10)$$

and constitutes the departing point for any study of particle diffusion and dispersion.

There are many proposals to model anomalous diffusion by means of generalized diffusion equations [24,27,34–38]. Despite the various models examined a general solution to the problem has not been found. Starting with a generalized fractional diffusion equation of the form

$$\frac{\partial^\beta P}{\partial t^\beta} = \mathcal{D} \frac{\partial^\alpha P}{\partial |x|^\alpha} + \frac{t^{-\beta}}{\Gamma(1-\beta)} \delta(x), \quad (11)$$

with $0 < \beta \leq 1$ and $0 < \alpha \leq 2$, different scenarios have been discussed in the literature. One such case is related to the so-called Lévy process, which can be obtained from Eq. (11) by setting $\beta = 1$, with $0 < \alpha \leq 2$. The solution to this initial value problem corresponds to the Lévy process (see, for example, Ref. [36]). Other cases deal with the problem of time-fractional and/or space-fractional diffusion equations (see, for example, Refs. [24,37]). In Eq. (11) the operator $\partial^\beta / \partial t^\beta$ is the fractional Riemann-Liouville time derivative of order β and $\partial^\alpha / \partial |x|^\alpha$ is the Riesz space-fractional derivative of order α . These fractional derivatives are integro-differential operators whose definition is given in [36,37]. A brief summary of these formulas is provided in the Appendix. The last term in Eq. (11) is the source term and depends on the initial conditions. Most of the studies use free boundary conditions and initial conditions centered on the origin, i.e., $P(x,0) = \delta(x)$, such that the Fourier-Laplace transforms of the Green functions [i.e., the solution for the $\delta(x)$ initial condition $P(x,0) = \delta(x)$] can easily be obtained. Of particular interest to this study is the case of $0 < \beta \leq 1$ and $\alpha = 2$, which corresponds to so-called fractal Brownian motion or the time-fractional diffusion equation. Following the results by Minardi *et al.* [34,35], Eq. (11) becomes equivalent to the following initial value problem:

$$\frac{\partial^\alpha P}{\partial t^\alpha} = \mathcal{D} \frac{\partial^2 P}{\partial x^2}, \quad (12)$$

where \mathcal{D} denotes a positive constant with dimensions $L^2 T^{-\alpha}$. Note that in Eq. (12) the time exponent β has been replaced by an order α (in the Caputo sense) with $0 < \alpha \leq 2$ (see the Appendix for the definition of the Caputo fractional derivative) [29,34]. A thorough explanation for the introduction of the Caputo fractional derivative in place of the more common Riemann-Liouville fractional derivative has been provided by Mainardi *et al.* [34]. A discussion of the convenience of replacing the integer order time derivative by a fractional derivative of the Riemann-Liouville, Weyl, Riesz, Grünwald, Caputo, or Marchaud type is beyond the scope of this paper; therefore this topic will not be presented here. The interested reader is referred to, e.g., Refs. [37,39] and references therein.

The solution of Eq. (12) with the initial condition $P(x,0) = \delta(x)$ is obtained by Fourier-transforming both sides of the equation with respect to x . After integration and inverse Fourier-transforming of the Green function, the solution is given by

$$P(\delta x, t) = \frac{1}{2\sqrt{\mathcal{D}t^\nu}} M(\zeta, \nu), \quad (13)$$

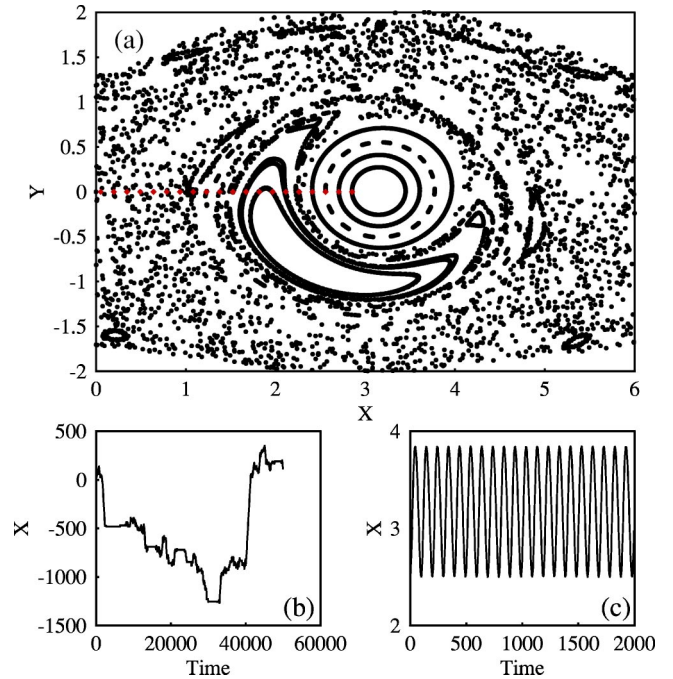


FIG. 4. Results of simulation for ten particle tracers advected by the Kelvin flow. (a) Poincaré section, (b) sample trajectory from the chaotic region, and (c) sample trajectory from the ordered region.

where $\nu = \alpha/2.0$ and $M(\zeta, \alpha)$ is a function of Wright type, defined by

$$M(\zeta, \nu) = \frac{1}{\pi} \sum_{n=0}^{\infty} \frac{(-\zeta)^{n-1}}{(n-1)!} \Gamma(n\nu) \sin(n\pi\nu), \quad (14)$$

with

$$\zeta = \frac{|x|}{\sqrt{\mathcal{D}t^\nu}}. \quad (15)$$

The classical Gaussian solution is recovered when $\nu = 0.5$. The properties of the $M(\zeta, \alpha)$ function are given in Refs. [34,36]. It can easily be shown that the variance associated with this PDF exhibits the time dependence $\sigma^2 \propto t^\nu$. The analytical solution in Eq. (13) is applied in Sec. IV to fit the PDF of particle displacements.

IV. RESULTS AND DISCUSSION

We begin by examining the kinematics (i.e., evolution of particle paths as a function of time). The tracer particle paths, which in this case coincide with the streamlines of the flows, follow from the solution of the system of equations describing the velocity fields indicated in Sec. II. The Poincaré sections in Figs. 4(a), 5(a), and 6(a), which provide a qualitative picture of the flows, agree closely with previous studies [6,7,16]. KAM tori (loci of quasiperiodic orbits about elliptic points) and cantori as well as quasiperiodic islands (cross sections of toroidal flow regions) are observed. Particle tracers that begin within the domain of an invariant torus remain confined on it, that is, KAM tori act as impermeable barriers to transport, therefore particles in this region never escape

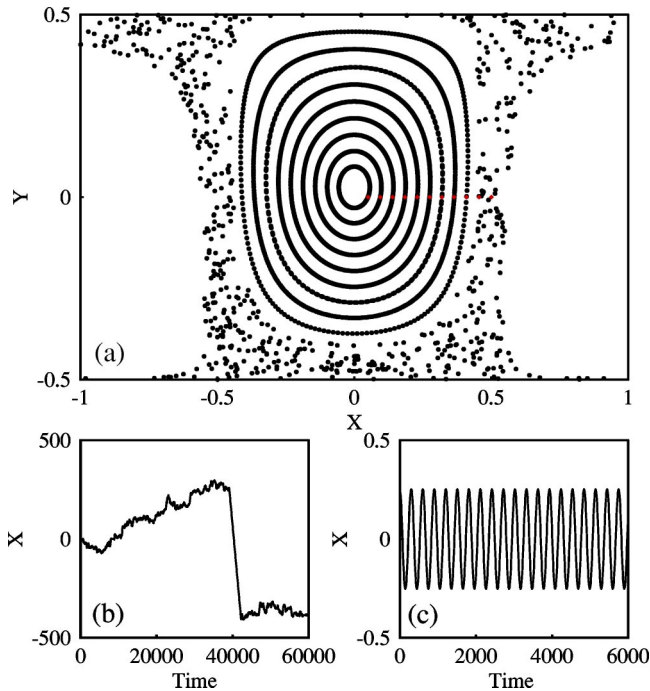


FIG. 5. Results of simulation for ten particle tracers advected by the Rayleigh-Bénard flow. (a) Poincaré section, (b) sample trajectory from the chaotic region, and (c) sample trajectory from the ordered region.

through their corresponding KAM torus. This has important consequences for transport (see, for example, Refs. [14,15,40]). The pattern of the trajectories is relatively simple within KAM tori, but becomes more complex as the chaotic region is approached. Cantori, unlike KAM tori, are only partial barriers to transport and therefore particles initially trapped in this regions eventually escape to explore other regions of the flow field [41]. The gaps between cantori are chaotic regions and islands of regular motion (unmixed regions). Islands of period 2, 3, and 4 can be found in these flows. Higher order islands may exist but are not resolved with the number of iterations and initial conditions used in this study.

Of particular interest to this study are the unbounded trajectories in the chaotic region, such as those plotted in Figs. 4(b), 5(b), and 6(b). Passive tracers undergoing these trajectories travel long distances in short period of times, with periods of trapping in the regular regions of the flow before moving to the next cell in the flow field—a well established characteristic of Lévy flights. The sticking process results in flights with a wide range of lengths and durations. A wide range of flights is possible depending on the location of the particle in the flow field. The chaotic character of these trajectories may be verified by demonstrating the sensitivity to initial conditions, characterized by the exponential divergence of nearby trajectories as measured by the estimation of the Lyapunov exponent.

Figures 4(c), 5(c), and 6(c) show particle trajectories in ordered regions of the flows. The oscillatory behavior stems from the quasiperiodic orbits which keep the particle trajectories confined within the KAM tori.

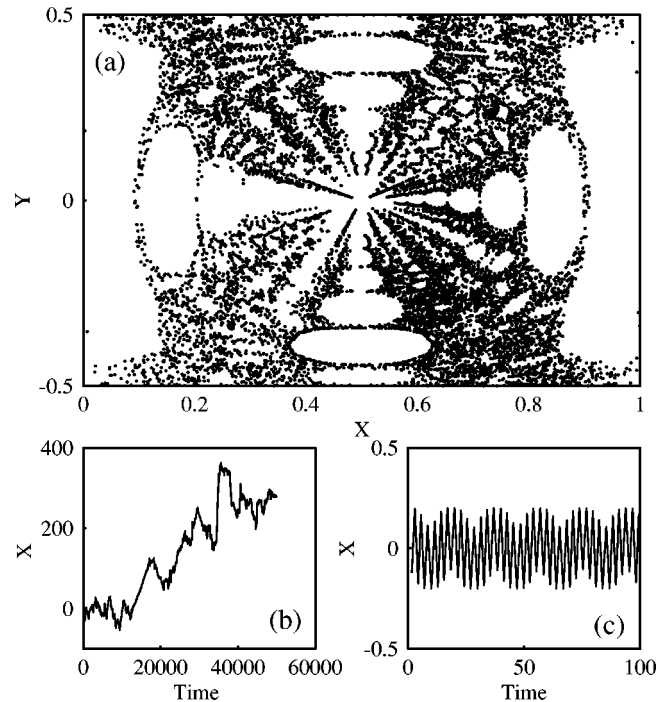


FIG. 6. Results of simulation for the advection of a single tracer in a 3D vortex flow. (a) Poincaré section, (b) sample trajectory from the chaotic region, and (c) sample trajectory from the ordered region.

We now examine the statistical behavior of the particle trajectories. Figures 7(a), 8(a), and 9(a) shows the corresponding evolution of the variance $\sigma^2(t) = \langle X^2 \rangle$ of particle displacements in the x direction for an ensemble of 100 particles that started uniformly distributed in the basic cell. $\langle \cdot \rangle$ denotes the ensemble average, $\delta x = x(t) - x(0)$, and $X = \delta x - \langle \delta x \rangle$. The profiles in Figs. 7(a), 8(a), and 9(a) show that the variance growth rate is superdiffusive for the Kelvin flow [Fig. 7(a)] and the three-dimensional vortex flow [Fig. 9(a)] with a characteristic exponent $\gamma > 1.0$, meaning that $P(\delta x, t)$ spreads faster than in a normal diffusive process. The superdiffusive behavior is essentially due to the trapping of the particle trajectories close to cantori or islands of regularity which are organized in self-similar structures. The variance growth for the Rayleigh-Bénard flow [Fig. 8(a)] indicates a normal diffusive process, with $\gamma \approx 1$. It is well established that the transport in the Rayleigh-Bénard flow follows a classical Gaussian behavior for most frequencies, but it is superdiffusive for well defined resonant frequencies [7]. In this particular simulation we used a frequency $f = 0.106$, which is known to generate superdiffusive behavior for particles in the chaotic region of the flow. However, the global behavior of the system is classical. For this specific case and with the number of particle tracers considered, the number of tracers undergoing long flights is not enough to dominate the statistics of the system and hence the growth of the variance scales with $\gamma \approx 1$. In panels (a) of Figs. 7–9, the filled symbols denote the numerical results, and the solid lines linear fits. These results are in agreement with previous investigations [6,10,33].

The probability density function for the spreading of 100

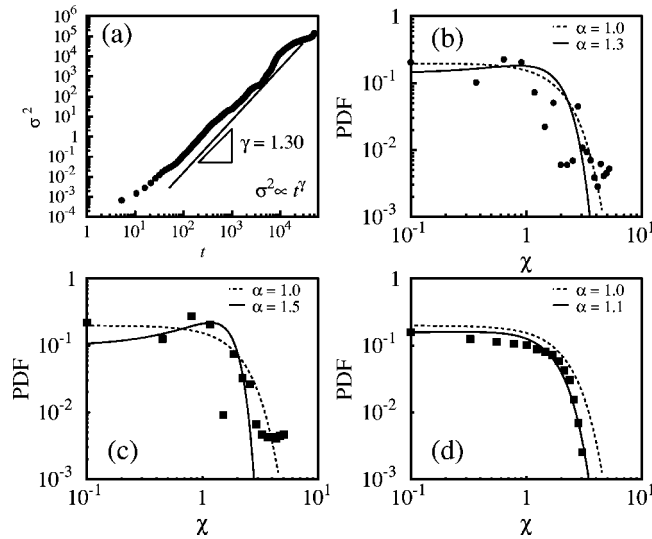


FIG. 7. Variance σ^2 and probability density function of particle displacements in the Kelvin cat eyes flow. (a) Variance growth; (b) global probability distribution function; (c) probability distribution from chaotic region; (d) probability distribution from ordered region. In panels (b), (c), and (d), the dashed and continuous lines represent the solution of Eqs. (13)–(15) of order α . The dashed line corresponds to $\alpha = 1$, which represents a Gaussian distribution. Parameter values for the simulation are $\epsilon = 0.1$, $\omega = 1.2$, $A = 0.8$.

tracers is shown as a function of the variable $\chi = X/t^\gamma$ in Figs. 7(b), 8(b), and 9(b) for the three flows considered in this study. The values of γ used in the determination of χ are the same as those found for the scaling of the variance in panels (a) of the corresponding figures. Some general comments are in order. The distributions are characterized by a peak which is shifted to nonzero χ values and by non-

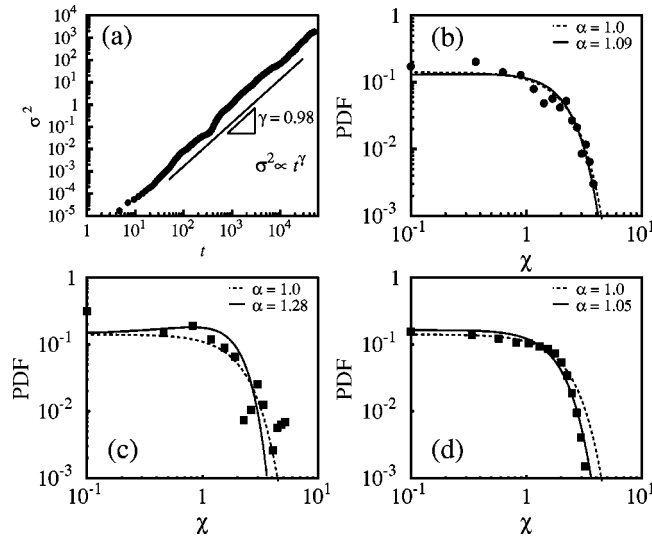


FIG. 8. Variance σ^2 and probability density function of particle displacements in the Rayleigh-Bénard flow. (a) Variance growth; (b) global probability distribution function; (c) probability distribution from chaotic region; (d) probability distribution from ordered region. Simulation parameters are $B = 0.1$, $a = d = 1.0$, $\lambda = 2d$, $\omega = 0.66$.

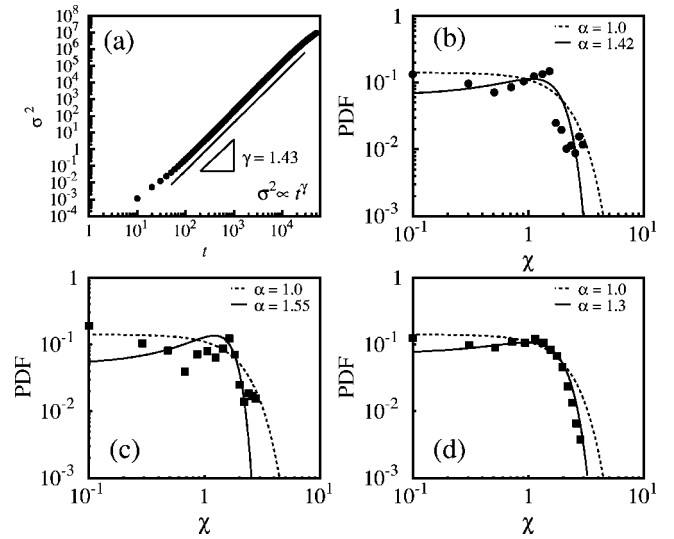


FIG. 9. Variance σ^2 and probability density function of particle displacements in the (3D) vortex flow. (a) Variance growth; (b) global probability distribution function; (c) probability distribution from chaotic region; (d) probability distribution from ordered region. Simulation parameters are $d_1/d_2 = 1.0$, $a_1/a_2 = 5.0$, $\lambda = 2.0$.

Gaussian tails. The curves as a whole display Gaussian and/or non-Gaussian behavior which is relatively well described by a time-fractional diffusion equation of order α . The non-Gaussian behavior of the tracer particle displacements is caused by the correlations in the Lagrangian velocity field created by the regular regions and the shear flow [10]. The global order of the time-fractional diffusion equation seems to be determined by two contributions. Here we investigate this observation by analyzing the particles in the chaotic regions of the flow independently from those in the ordered regions. In Figs. 7(c), 7(d), 8(c), 8(d), 9(c), and 9(d) the normalized PDFs for the chaotic and ordered regions are shown. The plots in panels (c) indicate that the PDF of particle displacements in the chaotic regions of the flow are non-Gaussian with orders $\alpha > 1.0$ in all cases. On the other hand, the plots in panels (d) which represent particle trajectories in the ordered regions of the flow show almost a Gaussian behavior with the order α closer to 1.

The dashed lines in panels (b), (c), and (d) of Figs. 7, 8, and 9 show the solution of the time-fractional diffusion equation [Eqs. (13)–(15)] with $\alpha = 1.0$ (Gaussian distribution) and the solid lines denote the predictions of the fractional equation of order $\alpha \neq 1$ (non-Gaussian distribution). The results show that particles in the chaotic regions are more likely to exhibit anomalous diffusion ($\alpha > 1$) while those in regular (ordered) regions of the flow field show a more classical Gaussian behavior ($\alpha \approx 1$). Plots of variance growth (not shown) for particles in the ordered region reveal a scaling exponent $\gamma \sim 1$. In general, each of the flows considered exhibits a significant anomalous diffusion behavior, indicating that the cantori barriers to the flow cause a significant trapping within the vortices. In all cases the figures show that the time-fractional equation provides a reasonable description of the probability distribution functions; however, some deviations exist at the extremes of the distribution. As

pointed out by Barkai [38] in his study of the foundations of the fractional diffusion equations, the fractional approach also has its limitations when compared with the classical diffusion approximation.

Based on his study Barkai found that the fractional approximation for decoupled fractional diffusion equations—the case considered in Eq. (11)—can break down at the origin $x=0$, and in general the convergence of the solution at $x \rightarrow 0$ can be extremely slow. There are also difficulties in predicting correctly the behavior of the high order moments and therefore the solution might not describe properly the tails of the Green function, i.e., $x \rightarrow \infty$. Similar observations have been made by Mainardi *et al.* [42]. These assertions seem to be confirmed by the results in Figs. 7, 8, and 9, where the core of the distribution is well described using the time-fractional diffusion equation but there is a systematic deviation at the extremes. The previous results show that for many flows a Lagrangian analysis based on the fractional diffusion equation may be applied to further extend the analysis based on classical approaches. It has been suggested by Castiglione *et al.* [33] that in the case of strong anomalous diffusion the equations describing the transport process at large scales and long times obey neither the classic Fickian behavior nor any other linear equation that involves temporal and/or spatial fractional order of the derivatives. However, the time-fractional diffusion equation, although still unable to exactly reproduce all the features of the PDF, provides the means to characterize qualitatively and quantitatively these kinds of flows.

V. CONCLUSIONS AND OUTLOOK

In this article the Lagrangian dynamics of particle tracers in two- and three-dimensional cellular flows, $N=O(100)$, has been analyzed. We find that the global behavior of the dispersion process can be understood by partitioning the system into two distinct regions: (1) classical (Gaussian) behavior resulting from the ordered regions of the flow field, and (2) non-Gaussian (anomalous) behavior resulting from the advection process in the chaotic regions of the flow. We calculated probability density functions for the displacements of particle trajectories in the chaotic and regular regions of cellular flows and show that the resulting distributions are well described by a time-fractional diffusion equation of order α , with $\alpha > 1.0$ in all cases. The analytical solution reproduces the basic features of the numerically determined PDFs. Our results support the notion that a fractional description is probably better than a classical one. However, neither approach seems to be accurate enough to be able to describe the entire range; further work on this topic is needed.

These results provide a glimpse as to how the dispersion of nonbouyant particles may occur and how this process can

be quantified; work in this direction is currently in progress. Preliminary experimental results by Abatan *et al.* [43] on the migration of particles and droplets in a cellular, multidirectional, viscous flow with finite fluid inertia indicate that, contrary to common perception, these vastly different “particles” can migrate across streamlines to position themselves in regular regions of the flow—regardless of their density—provided that the right inertial properties are selected. The migration processes of single particles and clusters reveal Lévy-like trajectories, with discrete trapping and flying events. These observations reinforce the existence of multiple equilibrium positions within simple laminar flows, as observed qualitatively in the Poincaré sections of the flow. It has been experimentally observed that the final and/or intermediate equilibrium positions of the particles coincide with the regular—ordered—regions of the flow.

ACKNOWLEDGMENTS

We wish to acknowledge the collaboration of Dr. J. J. McCarthy (University of Pittsburgh) for a careful reading of the manuscript and for his insight in clarifying some of the concepts. The support of the Research Center (School of Engineering, Universidad Militar Nueva Granada) is greatly appreciated.

APPENDIX

This section describes some basic formulas used in the text. More information on these and related subjects can be found in the references.

The Riemann-Liouville fractional derivative of order β , with $0 < \beta < 1$:

$$\frac{d^\beta}{dt^\beta} f(t) = \frac{1}{\Gamma(1-\beta)} \frac{d}{dt} \left[\int_0^t \frac{f(\tau)}{(t-\tau)^\beta} d\tau \right]. \quad (\text{A1})$$

The Riesz fractional derivative of order α , with $0 < \alpha < 2$:

$$\begin{aligned} \frac{d^\alpha}{dt^\alpha} f(x) &= \Gamma(1+\alpha) \frac{\sin(\alpha\pi/2)}{\pi} \\ &\times \int_0^\infty \frac{f(x+\xi) - 2f(x) + f(x-\xi)}{\xi^{1+\alpha}} d\xi. \quad (\text{A2}) \end{aligned}$$

The Caputo fractional derivative of order β , with $0 < \beta < 2$:

$$\frac{d^\beta}{dt^\beta} f(t) = \frac{1}{\Gamma(1-\beta)} \frac{d}{dt} \left[\int_0^t \frac{f(\tau)}{(t-\tau)^\beta} d\tau \right] - \frac{t^{-\beta}}{\Gamma(1-\beta)} f(0). \quad (\text{A3})$$

[1] H. Aref, *J. Fluid Mech.* **141**, 1 (1984).

[2] P. K. Newton and E. Meiburg, *Phys. Fluids A* **3**, 1068 (1991).

[3] V. Ganesan, M. D. Bryden, and H. Brenner, *Phys. Fluids* **9**, 1296 (1997).

[4] J. M. Finn, *Chaos* **12**, 508 (2002).

[5] H. Aref, *Phys. Fluids A* **3**, 1009 (1991).

[6] M. A. Fogleman, M. J. Fawcett, and T.H. Solomon, *Phys. Rev. E* **63**, 020101 (2001).

- [7] T. H. Solomon, A. T. Lee, and M. A. Fogleman, *Physica D* **157**, 40 (2001).
- [8] M. D. Bryden and H. Brenner, *J. Fluid Mech.* **379**, 319 (1999).
- [9] H. Aref, *Nature (London)* **401**, 756 (1999).
- [10] D. del Castillo-Negrete, *Phys. Fluids* **10**, 576 (1998).
- [11] T. H. Solomon and J. P. Gollub, *Phys. Rev. A* **38**, 6280 (1988).
- [12] T. H. Solomon and J. P. Gollub, *Phys. Fluids* **31**, 1372 (1988).
- [13] E. R. Weeks, Ph.D. thesis, University of Texas at Austin, 1997.
- [14] G. O. Fountain, D. V. Khakar, and J. M. Ottino, *Science* **281**, 683 (1998).
- [15] G. O. Fountain, D. V. Khakar, I. Mezic, and J. M. Ottino, *J. Fluid Mech.* **417**, 265 (2000).
- [16] Y. Tsega, E. E. Michaelides, and E. V. Eschenazi, *Chaos* **11**, 351 (2001).
- [17] J. B. Weiss, A. Provenzale, and J. C. McWilliams, *Phys. Fluids* **10**, 1929 (1998).
- [18] T. Dombre, U. Frisch, J. M. Green, M. Henon, A. Mehr, and A. M. Soward, *J. Fluid Mech.* **167**, 353 (1986).
- [19] K. Bajer and H. K. Moffatt, *J. Fluid Mech.* **212**, 337 (1990).
- [20] H. A. Stone, A. Nadim, and S. H. Strogatz, *J. Fluid Mech.* **232**, 629 (1991).
- [21] P. Ashwin and G. P. King, *J. Fluid Mech.* **338**, 341 (1997).
- [22] F. H. Ling, *Phys. Fluids A* **5**, 2147 (1993).
- [23] D. A. Benson, Ph.D. thesis, University of Nevada, 1998.
- [24] S. C. Lim and S. V. Muniandy, *Phys. Rev. E* **66**, 021114 (2002).
- [25] G. Drazer, H. S. Wio, and C. Tsallis, *Granular Matter* **3**, 105 (2001).
- [26] V. V. Kulish and J. L. Lage, *J. Heat Transfer* **122**, 372 (2000).
- [27] G. M. Zaslavsky, M. Edelman, and B. A. Niyazov, *Chaos* **7**, 159 (1997).
- [28] N. Laskin, *Physica A* **287**, 482 (2000).
- [29] E. Scalas, R. Gorenflo, and F. Mainardi, *Physica A* **284**, 376 (2000).
- [30] R. Camassa and S. Wiggins, *Phys. Rev. A* **43**, 774 (1991).
- [31] J. M. Ottino, *The Kinematics of Mixing: Stretching, Chaos, and Transport* (Cambridge University Press, New York, 1989).
- [32] T. H. Solomon, S. Tomas, and J. L. Warner, *Phys. Fluids* **10**, 342 (1998).
- [33] P. Castiglione, A. Mazzino, P. Muratore-Ginanneschi, and A. Vulpiani, *Physica D* **134**, 75 (1999).
- [34] F. Mainardi, P. Paradisi, and R. Gorenflo (unpublished).
- [35] R. Gorenflo and F. Mainardi, *Arch. Mech.* **50**, 377 (1998).
- [36] A. I. Saichev and G. M. Zaslavsky, *Chaos* **7**, 753 (1997).
- [37] R. Metzler and T. F. Nonnenmacher, *Chem. Phys.* **284**, 67 (2002).
- [38] E. Barkai, *Chem. Phys.* **284**, 13 (2002).
- [39] R. Hilfer, *J. Phys. Chem. B* **104**, 3914 (2000).
- [40] T. Makino, N. Ohmura, and K. Kataoka, *J. Chem. Eng. Jpn.* **34**, 574 (2001).
- [41] F. Sotiropoulos, Y. Ventikos, and T. C. Lackey, *J. Fluid Mech.* **444**, 257 (2001).
- [42] F. Mainardi, Y. Luchko, and G. Pagnini, *Frac. Calc. Appl. Anal.* **4**, 153 (2001).
- [43] A. A. Abatan, W. L. Vargas, E. Y. Marrero, and J. J. McCarthy (unpublished).